

Hiltunen, J., Suortti, T., Arvela, S., Seppä, M., Joensuu, R., and Hari, R. (2005). Diffusion tensor imaging and tractography of distal peripheral nerves at 3 T. *Clinical Neurophysiology*, 116: 2315-2323.

© 2005 Elsevier Science

Reprinted with permission from Elsevier.

Diffusion tensor imaging and tractography of distal peripheral nerves at 3 T

Jaana Hiltunen^{a,b,c,*}, Taru Suortti^{a,b}, Sakari Arvela^{a,b}, Mika Seppä^a,
Raimo Joensuu^b, Riitta Hari^{a,b,d,e}

^aBrain Research Unit, Low Temperature Laboratory, Helsinki University of Technology, P.O. Box 2200, 02015 Espoo, HUT, Finland

^bAdvanced Magnetic Imaging Centre, Helsinki University of Technology, P.O. Box 3000, 02015 Espoo, HUT, Finland

^cBrain and Work Research Centre, Finnish Institute of Occupational Health, Topeliuksenkatu 41 a A, 00250 Helsinki, Finland

^dDepartment of Clinical Neurophysiology, Helsinki University Central Hospital, 00290 Helsinki, Finland

^eNeuroscience Center, University of Helsinki, 00014 Helsinki, Finland

Accepted 14 May 2005

Abstract

Objective: We studied whether distal peripheral nerves could be imaged using quantitative diffusion tensor imaging (DTI) with a 3-T MRI scanner, and visualized using tractography.

Methods: Altogether 6 healthy subjects were studied. The diffusion was quantified with apparent diffusion coefficient (ADC) and fractional anisotropy (FA) maps, and the direction of main diffusivity was visualized with color-coded orientation maps and tractography.

Results: We present the first DTI and tractography results of human distal peripheral nerves. The courses of median, ulnar, and radial nerves in the upper limb and of tibial and peroneal nerves in the lower limb were first analyzed quantifying ADC and FA, and then visualized in 3D with tractography. Tractography illustrated nicely the 3D courses of both upper and lower limb nerves which were reliably distinguished from the surrounding muscle tissue and ligaments.

Conclusions: Quantitative DTI and tractography can be used to image and visualize distal peripheral nerves.

Significance: DTI is a quantitative method that could provide useful information for the diagnosis and follow-up of nerve lesions, entrapments, and regeneration. Peripheral nerves as well-delineated structures also containing abundant branching into bundles of different diameters, could be used as ‘living phantoms’ for testing and validating different tractography methods.

© 2005 International Federation of Clinical Neurophysiology. Published by Elsevier Ireland Ltd. All rights reserved.

Keywords: Diffusion tensor imaging; Tractography; Distal peripheral nerves

1. Introduction

Diffusion tensor imaging (DTI), based on magnetic resonance imaging (MRI), reveals microstructure of tissues by monitoring the random movement of water molecules (Basser et al., 1994; Le Bihan, 1995). DTI is especially advantageous for tissues containing organized microstructure, such as white matter tracts in the brain. In such fiber

bundles, water molecules move more in the direction along the fibers than to other directions. This inhomogeneity of diffusion, called anisotropy, can be quantified with diffusion tensor imaging. The accuracy of diffusion tensor measurements with echo-planar imaging (EPI) is limited by the image resolution, which in human brain imaging is typically 2–3 mm within a slice of 3–5 mm thickness. Such data are sufficient for identifying and visualizing bundles of nerve fibers.

The orientation and 3D course of white matter tracts can be visualized with tractography (Basser et al., 2000; Jones et al., 1999b; Mori et al., 1999; Parker et al., 2002, 2003; Poupon et al., 2001; Tench et al., 2002). For that purpose,

* Corresponding author. Address: Advanced Magnetic Imaging Centre, Helsinki University of Technology, P.O. Box 3000, 02015 Espoo, HUT, Finland. Tel.: +358 9 451 6159; fax: +358 9 451 6172.

E-mail address: jaana@neuro.hut.fi (J. Hiltunen).

diffusion tensor, describing the diffusion within the voxel, is first calculated using the diffusion-weighted images obtained with different diffusion gradient orientations (Basser et al., 1994). The eigenvalue decomposition of diffusion tensor is computed as well, and the direction of the eigenvector corresponding to the largest eigenvalue (principal eigenvector), reflecting the direction of largest diffusivity, is then considered to be parallel to the fibers (Basser et al., 1994).

The main applications of DTI so far have been in studies of white matter structures of the human brain (Gillard et al., 2001; Pierpaoli et al., 1996; Shimony et al., 1999; Wieshmann et al., 1999). Recently, DTI has been used also for imaging of spinal cord (Clark and Werring, 2002; Wheeler-Kingshott et al., 2002), kidneys (Ries et al., 2001), heart (Dou et al., 2002; Reese et al., 1995), muscles (Sinha and Yao, 2002), and as an example of proximal peripheral nerves, the human sciatic nerve in the thigh (Skorpil et al., 2004).

In studies of the brain's white matter tracts, the main rotationally invariant parameter images are (i) the apparent diffusion coefficient (ADC) that describes the mean diffusivity, and (ii) the anisotropy indices, such as the fractional anisotropy (FA) that describes the degree of anisotropy in the tissue (Basser and Pierpaoli, 1996). Tractography has been widely applied in brain research (Bammer et al., 2003; Catani et al., 2002; Jones et al., 2002; Masutani et al., 2003; Melhem et al., 2002), but only to a limited extent to visualize other anatomical structures (Skorpil et al., 2004; Wheeler-Kingshott et al., 2002).

The first MRI neurography of human peripheral nerves included images obtained with T2-weighted fat-saturated fast spin-echo (FSE) sequence (Filler et al., 1993), and later also T1-weighted sequences were used (Filler et al., 1996). Recent clinical MRI studies of peripheral nerves typically used T1-weighted spin-echo sequences and T2-weighted short-tau inversion recovery (STIR) or fat-saturated FSE sequences (Grant et al., 2004; Jarvik and Yuen, 2001; Jarvik et al., 2000, 2004). However, the analysis of such data has been qualitative and subjective, based on visual inspection of the images. Our aim was to study the feasibility of DTI and tractography for visualization of distal peripheral nerves, imaged with a 3-T MRI scanner. As a clear improvement to earlier MRI methods applied to peripheral nerves, DTI is a quantitative method and enables more objective analysis. We quantified the diffusion with ADC and FA parameter images and visualized with color-coded orientation maps, but definitely the best visualization was obtained with tractography that nicely illustrated the 3D course of both upper and lower limb distal peripheral nerves.

We envision that reliable DT imaging of peripheral nerves might provide a new clinical tool for the diagnosis and follow-up of entrapments, trauma and regeneration of peripheral nerves. In addition, because peripheral nerves, at least in healthy subjects, can be separated well from other

surrounding tissues, they might also be used as 'living phantoms' for testing different DTI pulse sequences, imaging parameters, and tractography algorithms. The advantage is the clear delineation of the peripheral nerves compared with the tight package of different fiber tracts in the brain's white matter.

2. Methods

2.1. Subjects

Altogether 6 healthy members of the laboratory personnel were studied (3 males, 3 females; age range 22–36 years). Nerves at the ankle, calf (10–20 cm distal to poplitea), and knee were studied in 3 subjects, and nerves at the wrist in 4 subjects (one subject participated in both upper and lower limb measurements). Subjects were studied after informed consent, and the study had a prior approval by the local ethics committee.

2.2. Imaging

The MR images were acquired with Signa VH/i 3.0T MRI scanner (General Electric, Milwaukee, WI) using a quadrature receiving-and-transmitting extremity coil (IGC-Medical Advances, Inc., WI) for imaging of the ankle, calf, and knee, and a quadrature receiving-only coil for the wrist. The wrist coil (IGC-Medical Advances, Inc., WI), originally designed and tuned for a 1.5-T GE scanner, was retuned for 3 T (www.ami.hut.fi/facilities/AMIwrist.html). The MRI system's maximum field gradient amplitude was 40 mT/m, with slew rate 150 T/m/s.

During the scanning session, the coil was positioned to the center of the magnet bore. Although this positioning produced small discomfort for the subject, the quality of the echo-planar images (EPI) was then significantly better than when the coil was clearly on the right or left side, as is usual during anatomical imaging. The subject's right upper or lower extremity was positioned to the coil and immobilized with cushions, sandbags, and bandages. For imaging of the wrist, the subject was in the scanner in prone position (head first, hand up) and supine for lower limb imaging (feet first).

We used a spin-echo-based single-shot echo-planar sequence with diffusion sensitizing gradients positioned symmetrically with respect to a 180° refocusing pulse (Stejskal and Tanner, 1965). The sequence had a slice-selective spectral-spatial excitation pulse to suppress the signal of fat. The *b*-value, controlling the diffusion weighting, was 1000 s/mm². In addition to T2-weighted EPI images (*b*=0 images), 13 different diffusion gradient orientations (the maximum within the scanner database constraints) were selected, distributed evenly to the surface of the unit sphere (www.research.att.com/~njas/electrons); see also Jones et al. (1999a), Le Bihan et al. (2001), and Skare et al. (2000) for selecting evenly spaced gradient

Table 1
Normalized diffusion gradient orientations

Image volume	Gradients		
	x	y	z
1	0	0	0
2	-0.754	0.173	-0.633
3	0.330	-0.372	0.867
4	-0.533	-0.459	0.711
5	-0.687	-0.708	-0.163
6	-0.321	0.942	-0.101
7	0.618	0.786	-0.018
8	0.019	0.576	0.817
9	0.311	-0.949	0.051
10	-0.883	0.314	0.350
11	-0.038	-0.536	-0.843
12	0.184	0.469	-0.864
13	0.937	0.004	0.350
14	0.814	-0.236	-0.531

orientations. Table 1 shows our normalized diffusion gradient orientations.

Prior to DTI, high-order shimming with 28-cm field of view (FOV) was applied to reduce the inhomogeneities of the main magnetic field in the imaging area. Diffusion tensor data were acquired from 17 to 23 contiguous axial slices, each 3.5 mm thick. Echo time (TE) was set to minimum, i.e. 82–86 ms, depending on the imaging parameters (see Table 2 for details of sequence parameters). Number of excitations (NEX) was 3–4 to obtain a reasonable signal-to-noise ratio for image analysis.

T2*-weighted anatomical images were obtained, from the same anatomical locations as diffusion images, with a gradient-echo sequence to provide more detailed anatomical information. The imaging parameters were: repetition time (TR) 450–480 ms, TE = 15 ms, flip angle 20°, matrix size 256 × 256, NEX = 2, slice thickness 3.5 mm, without spacing between slices.

2.3. Data analysis

The quality of diffusion-weighted images, and the effect of distortions and artifacts on the parameter images were visually inspected on the scanner console and with post-processing software (see below). Furthermore, the quality of tractography was checked by comparing the tracts with the known anatomical structure of nerve bundles, and

Table 2
DT-sequence parameters in different anatomical areas

Parameter	Knee	Ankle	Wrist
Number of slices	23	23	17
FOV (cm)	14–16	12	10
Matrix	96 × 96	96 × 96	64 × 64
In-plane resolution (mm)	1.46–1.67	1.25	1.56
TR (ms)	7000	7000	5000
TE (ms)	83.9–82.0	86.2	83.5
Scanning time for 1 NEX (min:s)	01:38	01:38	01:10

by the length of fiber tracts that the post-processing softwares were capable to reconstruct. The images showed no severe distortions or artifacts, and therefore, post-processing correction methods were not used. As an example, Fig. 1A shows the T2-weighted EPI image ($b=0$) for knee.

The maps for apparent diffusion coefficient (ADC), fractional anisotropy (FA), and color-coded direction maps, as well as tractography images were computed with dTV1.5 software (Image Computing and Analysis Laboratory, Department of Radiology, The University of Tokyo Hospital, Japan; www.ut-radiology.umin.jp/people/masutani/dTV.htm), and viewed with Volume-One software (www.volume-one.org). ADC, describing the mean diffusivity, is a measure of diffusion magnitude. FA is a rotationally invariant scalar parameter describing the anisotropy degree of tissue. FA is scaled to obtain values between 0 and 1, where 0 represents isotropic diffusion and value 1 the complete anisotropy. In the color-coded maps, the principal eigenvector is presumed to represent the fiber direction in the voxel. The components of principal eigenvector are assigned to different colors (typically red, green, and blue), and the resulting image is weighted by values of FA image to exclude the tissues with isotropic diffusion. For details of color-coded map representation of tract direction, see e.g. Pajevic and Pierpaoli (1999).

The software that we used applied the tractography method of Masutani et al. (2003). Diffusion tensor was calculated for each voxel using the measured diffusion-weighted images, and further diagonalized to obtain eigenvalues and eigenvectors. The eigenvector corresponding to the largest eigenvalue was assumed to represent the fiber direction in the voxel. We used one ROI (region of interest) technique, by choosing a seed ROI through which the fibers were tracked. The nerve of interest was first approximately identified from anatomic gradient-echo images, and a freehand ROI, larger than the nerve diameter, was positioned to the corresponding location in the T2-weighted EPI image ($b=0$ image of diffusion series). The FA and color-coded maps were used to verify the position of ROIs on the nerves of interest. The maps were especially useful in subjects whose wrist was bent during the scanning, and therefore, tractography was more challenging. Tracking of the fiber tract stopped when the FA value of the voxel fell below 0.3 in foot and below 0.4 in wrist; these values were assumed to indicate that tracking had reached tissue outside the nerve. For several ROIs positioned in the nerve or in areas near the nerve, different FA threshold values and tract lengths were tested in tractography to distinguish nerve from muscle fibers and ligaments.

The mean ADC values and maximum FA values were measured from the ROIs used for tractography. The variation of ADC values was small, and therefore mean ADC described well enough the mean diffusivity within the ROI. FA values showed larger variation particularly so that low values were always obtained at

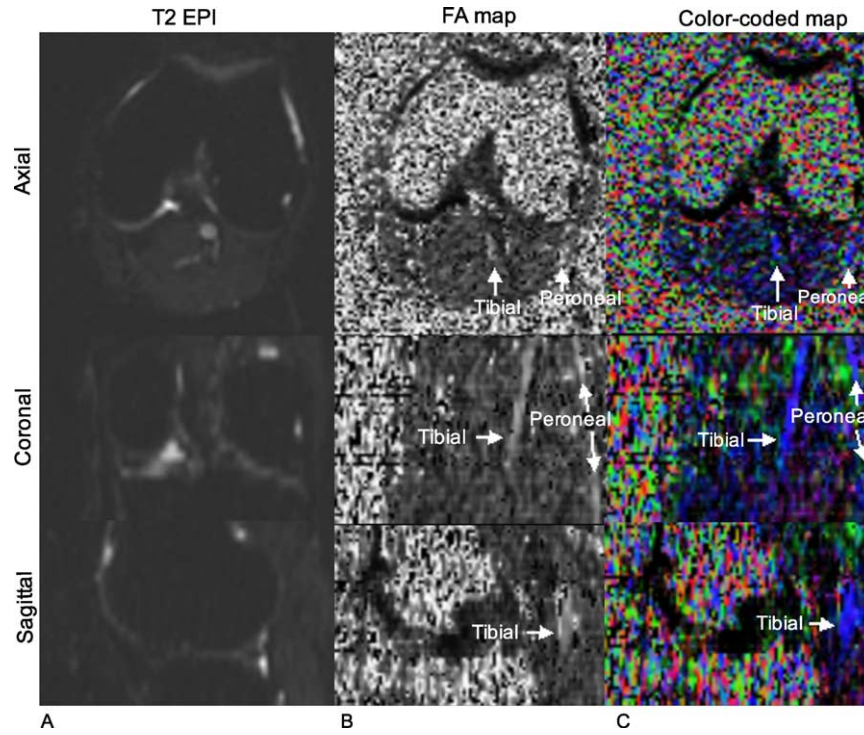


Fig. 1. Axial (top), coronal (middle) and sagittal (bottom) views of right knee of one subject: (A) T2-weighted EPI image ($b=0$ image), (B) fractional anisotropy (FA) image, and (C) color-coded direction map. The blue color indicates nerve, i.e. a structure with oriented diffusion in distal proximal direction.

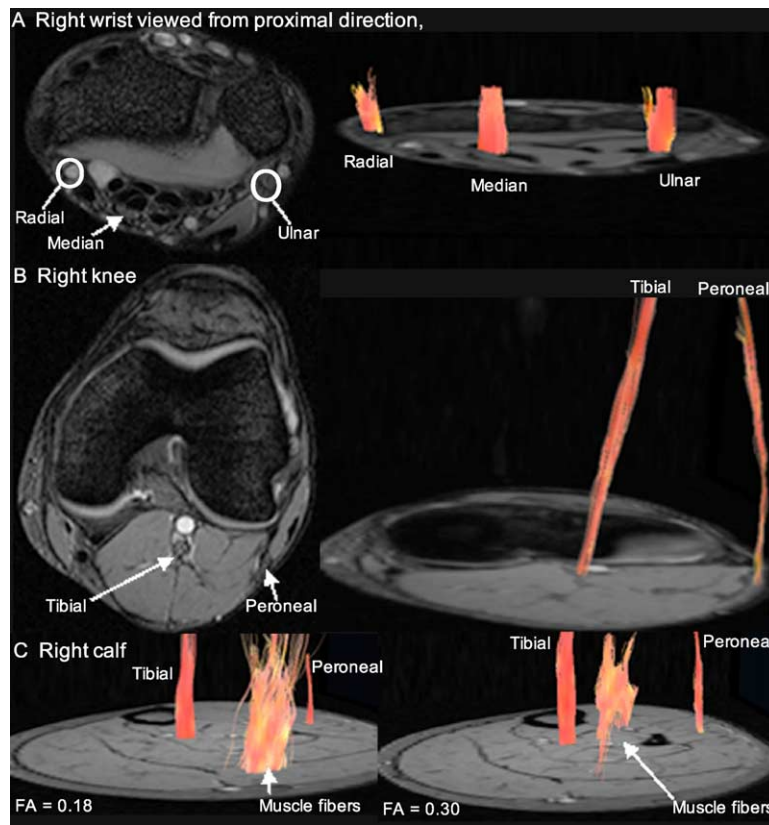


Fig. 2. Tractography of peripheral nerves of the right wrist imaged with diffusion tensor imaging, and the corresponding anatomic images showing the nerves: (A) median, ulnar, and radial nerve of wrist ($FA > 0.4$), (B) back view of tibial and peroneal nerve in knee ($FA > 0.3$), and (C) tibial and peroneal nerve of calf (long tracts), and muscle fibers with $FA > 0.18$ (left), and $FA > 0.30$ (right), respectively.

the edge of nerves, probably due to partial volume effects; the upper range of FA values increased with nerve size.

To increase the reliability and weight of the results, tractography for one subject was also performed with our own software that uses the algorithm of Westin et al. (2002). ROIs (radius 1 mm) were selected for tibial and peroneal nerves on the basis of the anatomical images, and fiber tracking was launched at 0.2 mm spacing inside the ROIs as long as FA was above 0.4 at each considered starting point. The fiber tracking was terminated when the FA fell below 0.3. The software can visualize the tracts with any volumetric data, e.g. with anatomical images, and with 3D structures segmented from such data. The user can interactively control the views and apply multiple cutting planes to inspect complex data sets.

3. Results

3.1. Apparent diffusion coefficient and fractional anisotropy

The magnitude of diffusion, quantified by the apparent diffusion coefficient (ADC), was rather similar in all subjects. For the lower-limb nerves of the 3 subjects, the mean ADC values within the ROI varied from 0.97×10^{-3} to 1.56×10^{-3} mm²/s, as is illustrated in Table 3. At the wrist, the corresponding mean ADC values for 4 subjects varied from 0.71×10^{-3} to 1.36×10^{-3} mm²/s (see Table 4). There were no significant differences in the ADC values between the nerves.

Fig. 1B and 1C show FA maps and color-coded orientation maps for right knee of one subject. Although both tibial and peroneal nerves are visible to an experienced examiner in the coronal images, the maps are rather difficult to interpret, especially compared with the tractography results shown below (Figs. 2 and 3). These maps were, however, useful for positioning the ROIs for tractography.

The maximum FA values tended to covary with the thickness of the nerve, being highest for tibial nerve at

Table 4
Mean ADC and maximum FA values for nerves in wrist

Nerve	Subject number	Max FA	Mean ADC ($\times 10^{-3}$ mm ² /s)
Median	2	0.89	0.94
	4	0.73	1.11
	5	0.74	1.02
	6	0.69	1.36
Ulnar	2	0.59	1.06
	4	0.62	1.04
	5	0.78	1.35
	6	0.72	0.95
Radial	2	0.64	1.01
	4	0.62	0.87
	5	–	–
	6	0.30	0.71

the knee and smallest for radial nerve (see Tables 3 and 4). The peroneal nerve at the knee and the tibial nerve at the ankle are of approximately the same size, and they also had rather similar maximum FA values (see Table 3). In the two subjects with lower maximum FA value for median than ulnar nerve, the median nerve was very flat within FA measurement area.

3.2. Tractography

Figs. 2 and 3 show tractography results for upper and lower limb nerves. Fig. 2A illustrates the median, ulnar, and radial nerves at the level of the right wrist; all bundles are nicely tracked and correspond well to the known anatomy: median nerve at the volar side of the wrist under the main tendons and ulnar nerve on the ulnar volar side of the wrist. In one of the 4 subjects, the radial nerve, which runs very superficially just under the skin on the radial side of the wrist, was not detected.

Fig. 2B shows tractography of the tibial and peroneal nerves at the level of the right knee, with nicely discernible bundles, corresponding to the known anatomy: the tibial nerve in the middle of poplitea behind the knee and the peroneal nerve at the lateral side, rather superficially. In the ankle area, the tibial nerve was still reliably seen in the inner side of the ankle, but the distal peroneal nerve on the metatarsus was not detected in any of the subjects.

Fig. 3 visualizes the right knee of one subject with our home-made software, with the tibial and peroneal nerves shown in relation to anatomical MRI data and structures segmented from those anatomical images.

3.3. Distinguishing the nerves from ligaments and muscles

Fig. 2C shows the tractography in right calf area, about 10 cm distal to the knee, with two FA thresholds. With a low threshold (FA = 0.18), both nerve fibers and muscle fibers are seen; the latter ones form a bundle of larger diameter and different shape. With a more stringent threshold (FA = 0.3),

Table 3
Mean ADC and maximum FA values for tibial and peroneal nerves in lower limb

Nerve and anatomical area	Subject number	Max FA	Mean ADC ($\times 10^{-3}$ mm ² /s)
Tibial (knee)	1	0.89	1.05
	2	0.85	1.15
	3	0.85	1.19
Peroneal (knee)	1	0.61	1.24
	2	0.80	1.06
	3	0.79	0.97
Tibial (ankle)	1	0.73	1.56
	2	0.79	1.11
	3	0.70	1.11

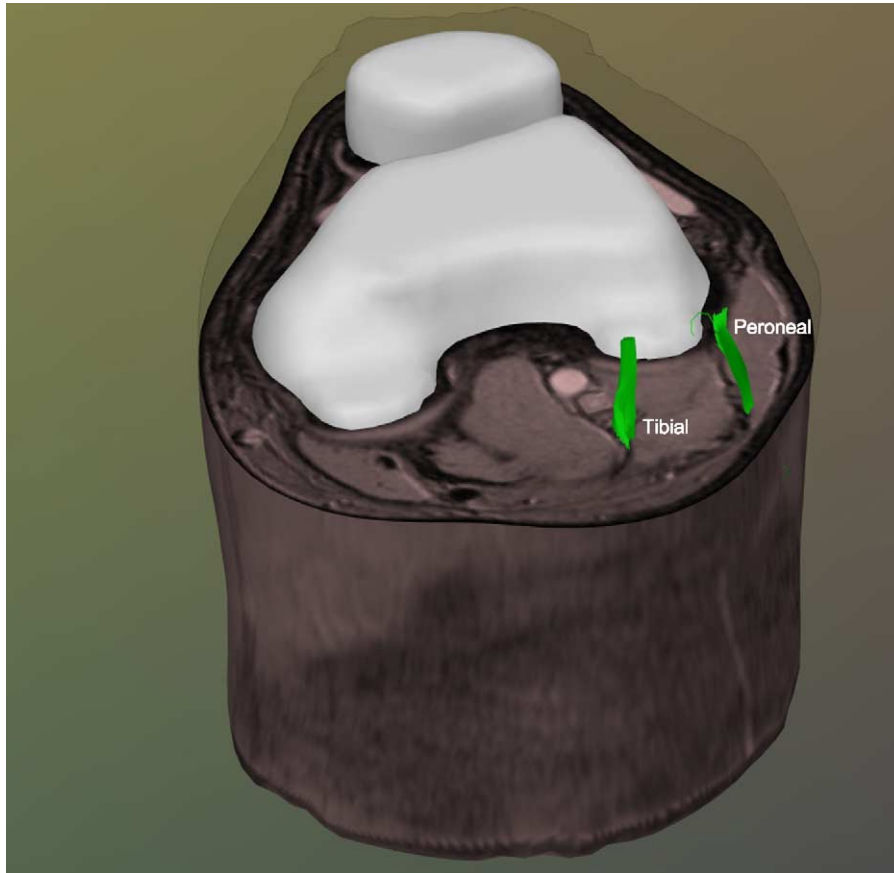


Fig. 3. Visualization of tibial and peroneal nerves of right knee region traced with our home-made software utilizing the tractography algorithm of Westin et al. (2002).

the muscle fibers are short bundles with high anisotropy, whereas the nerves are still seen as long fiber bundles. Similarly, the ligaments in the joint areas sometimes showed high anisotropy, but for short distances only and were thus easily separated from nerve fibers. At the wrist, threshold $FA = 0.4$ was suitable for detecting the nerves and for excluding the anisotropy originating from ligaments.

4. Discussion

We have demonstrated that the course of human distal peripheral nerves, i.e. the median, ulnar, and radial nerves at the wrist, the tibial and peroneal nerves at the knee, and the tibial nerve at ankle can be reliably imaged using diffusion tensor imaging (DTI) at 3 T, quantified with apparent diffusion coefficient (ADC) and fractional anisotropy (FA), and visualized in 3D using tractography. These nerves and anatomical areas were chosen since they are frequent sites of nerve entrapments. Our tractography results corresponded well to the known anatomy of the nerves.

To increase the reliability and to improve the interpretation of DTI results, ADC and FA maps, together with color-coded direction maps, were defined. In our healthy

subjects, ADC maps were of limited value since the tissue contrast between nerves and surrounding tissues is poor, similarly as is with tissue contrast between gray and white matter in the healthy brain. We therefore reported ADCs as individual mean values instead of maps. However, similarly as with brain lesions, ADC maps could be valuable when studying lesions in peripheral nerves.

The reported ADC and FA values were measured within the ROI that was used in tractography. The between-subject differences in mean ADC and maximum FA were rather small. However, maximum FA values tended to covary with nerve size, being the largest for the tibial nerve at the knee, and the smallest for the radial nerve at the wrist. This difference could reflect more compact tissue structure in larger nerves. On the other hand, possible partial volume effect would affect more smaller nerves, thereby causing lower FA values. In future patient studies, diffusivities along principal diffusion directions could provide additional information about the magnitude of diffusion, together with mean diffusivity quantified by ADC.

Before starting this study, we were afraid that anisotropy of other tissues, such as of the surrounding skeletal muscles and ligaments, could hinder the detection of the nerve or confuse the tractography results. However, the nerves were reliably distinguished from muscles/ligaments in

tractography on the basis of bundle size (diameter and length) and the degree of anisotropy. The fiber bundles in muscles are larger in diameter and considerably shorter than the fiber tracts of nerves. The ligaments can show high anisotropy, but were not problematic in the present study.

Basically, tractography is a segmentation method for the volumetric tensor data, just like 3D region growing is for volumetric scalar data, i.e. for T1- and T2-weighted images. According to our own experience, peripheral nerves cannot be distinguished clearly enough from the surrounding tissues in T1- and T2-weighted images. Therefore, automatic tracing with thresholds and 3D region growing would not reliably find them. Moreover, T1- and T2-images do not contain ‘direction’ information and thus 3D region growing expands to all directions equally, and easily escapes from the nerve structures. Instead, DTI data contain the direction information and consequently allow more robust nerve tracking.

4.1. Methodological considerations

The crucial parameter in DTI, and especially in tractography, is the signal-to-noise ratio (SNR). For imaging of distal peripheral nerves, the voxel size has to be small enough to enable reasonable resolution and to reduce the partial volume effect, but large enough to assure reasonable signal level. Our voxel sizes gave in-plane resolution of 1.6–2.8 mm² with 3.5 mm slice thickness, and together with chosen parameters provided sufficient SNR. The mean transectional area of the median nerve at the wrist, quantified in healthy subjects from 3-T MR images, is 10 mm² at the level of pisiform bone (Monagle et al., 1999).

In one subject, the radial nerve was not detected at the wrist. Since the radial nerve is thin and very superficial, even a slight geometrical distortion could have prevented the tracking. Furthermore, the nerve easily moves in the subcutis, and therefore, a small wrist flexion could have affected much more the position of the radial than the median and ulnar nerves. Moreover, anomalous hand innervation would result in deviations from textbook anatomy. At the ankle, we did not detect the thin and superficially located peroneal nerve, possibly due to small distortions or because the distal peroneal nerve branches into several thinner fiber bundles, and because it makes a sharp angle in the ankle area.

Firm fixation of joint area was extremely important to avoid movement during the imaging. We also found that wrist and knee should be supported well to avoid sharp bending in joints. Cushions, sandbags, and bandages were not always sufficient for support, and fiber tracking sometimes terminated obviously because of sharp bending of the wrist. However, tractography was not completely hampered even in these cases; instead, the nerves were tracked in several parts. In the future clinical studies,

positioning will be even more crucial, since the possible pathology has to be surely assigned to a nerve lesion.

If clinical applications of peripheral nerve DTI would emerge (as suggested below), attention should also be put to feasible coil configurations. If the site of a nerve lesion is not well known in advance, and if the coil dimensions limit the size of the imaging area, the positioning of the limb to the coil has to be planned carefully, or the limb has to be imaged in several parts. The imaging area with less than 25% intensity variation was for our wrist coil 25 mm × 39 mm × 44 mm in the volar–dorsal, left–right, and proximal–distal directions; for extremity coil the corresponding volume was 103 mm × 100 mm × 122 mm. The rather small diameter of wrist coil limits imaging of broader parts of the forearm, whereas the larger-diameter extremity coil provides wider anatomical coverage in proximal–distal direction.

4.2. ‘Living phantoms’

Tight package of different fiber tracts in the brain’s white matter and branching of neural fiber bundles cause difficult problems in brain DTI studies, and post-mortem histology continues to be the only known method for validation of the results. Some phantoms or calibration systems would be required for evaluation of the accuracy of the tractography algorithms. As was shown in the present study, DTI can separate fiber bundles of peripheral nerves well from the surrounding tissues, and supporting information can be obtained from anatomical MR images. As a proposition, peripheral nerves could be used as ‘living phantoms’ for testing and validating different DTI pulse sequences, imaging parameters, and tractography algorithms. Although peripheral nerves are usually quite simple linear structures, their diverging (and converging) branching into nerve bundles of different diameters is challenging enough for testing complex algorithms used for tractography.

4.3. Potential clinical uses

Peripheral nerves are surrounded by other types of tissues, such as ligaments and muscles, and our present data demonstrate that tractography is a much more powerful tool than are anisotropy maps in the visualization of the course of the nerve. Proper anatomic MR images, combined with the ADC, FA and color-coded direction maps are, however, valuable as they increase the reliability of tractography results. Such results are potentially clinically useful in the diagnosis and follow-up of diseases and lesions of peripheral nerves.

ADC is a quantitative parameter, independent of magnetic field strength, and it has been used for follow-up of patients with brain pathologies (Hein et al., 2004; Weber et al., 2000), as well as in patients with brain inflammation, swelling and cell necrosis due to demyelination

(Wheeler-Kingshott et al., 2003). We envision similar clinical application for studies of peripheral nerves.

Typical MRI finding in a nerve lesion is hyperintensity in T2-weighted STIR-images (Grant et al., 2002), which, however, is not lesion-specific and sometimes even appears in healthy nerves (Jarvik and Yuen, 2001). In carpal tunnel syndrome, signal intensities may be near normal at the point of maximal compression of median nerve (Jarvik and Yuen, 2001). Instead, diffusion-based imaging might be useful in pinpointing either decrease of water content or swelling due to compression at the site of the lesion.

Injuries of peripheral nerves, such as trauma and entrapments are often diagnosed and monitored by electrophysiological nerve conduction and electromyographic methods. However, after the correction surgery of a damaged nerve, it takes a long time until the electrical signal re-appears. It would therefore be interesting to see whether the regeneration of nerve could be monitored by DTI and tractography to provide information about the early phase of recovery. Although tractography is just one method to visualize the 3D course of nerves, DTI as a quantitative method could provide important information about the site of swelling and loss of water due to nerve lesion or entrapment. Clinical applications of DTI and tractography could be started from clear pathologies of peripheral nerves, preferably in combination with electrophysiological measurements.

Acknowledgements

This study was financially supported by the Academy of Finland, Louis-Jeantet Foundation (Switzerland), and Jenny and Antti Wihuri Foundation (Finland). We gratefully acknowledge the DTI sequence and recon code from Drs Michael Moseley and Gary Glover, supported by the NIH NCRG grant 'Stanford Center for Advanced Magnetic Resonance Technology', P41 RR09784 (PI: G. Glover). We thank Y. Hlushchuk for help in the image analysis, M. Kattelus for technical assistance during the recordings, and J. Numminen for discussions.

References

- Bammer R, Acar B, Moseley ME. In vivo MR tractography using diffusion imaging. *Eur J Radiol* 2003;45:223–34.
- Basser PJ, Pierpaoli C. Microstructural and physiological features of tissues elucidated by quantitative-diffusion-tensor MRI. *J Magn Reson B* 1996; 111:209–19.
- Basser PJ, Mattiello J, LeBihan D. MR diffusion tensor spectroscopy and imaging. *Biophys J* 1994;66:259–67.
- Basser PJ, Pajevic S, Pierpaoli C, Duda J, Aldroubi A. In vivo fiber tractography using DT-MRI data. *Magn Reson Med* 2000;44: 625–32.
- Catani M, Howard RJ, Pajevic S, Jones DK. Virtual in vivo interactive dissection of white matter fasciculi in the human brain. *Neuroimage* 2002;17:77–94.
- Clark CA, Werring DJ. Diffusion tensor imaging in spinal cord: methods and applications—a review. *NMR Biomed* 2002;15:578–86.
- Dou J, Reese TG, Tseng WY, Wedeen VJ. Cardiac diffusion MRI without motion effects. *Magn Reson Med* 2002;48:105–14.
- Filler AG, Howe FA, Hayes CE, Kliot M, Winn HR, Bell BA, Griffiths JR, Tsuruda JS. Magnetic resonance neurography. *Lancet* 1993;341: 659–61.
- Filler AG, Kliot M, Howe FA, Hayes CE, Saunders DE, Goodkin R, Bell BA, Winn HR, Griffiths JR, Tsuruda JS. Application of magnetic resonance neurography in the evaluation of patients with peripheral nerve pathology. *J Neurosurg* 1996;85:299–309.
- Gillard JH, Papadakis NG, Martin K, Price CJ, Warburton EA, Antoun NM, Huang CL, Carpenter TA, Pickard JD. MR diffusion tensor imaging of white matter tract disruption in stroke at 3 T. *Br J Radiol* 2001;74: 642–7.
- Grant GA, Britz GW, Goodkin R, Jarvik JG, Maravilla K, Kliot M. The utility of magnetic resonance imaging in evaluating peripheral nerve disorders. *Muscle Nerve* 2002;25:314–31.
- Grant GA, Goodkin R, Maravilla KR, Kliot M. MR neurography: diagnostic utility in the surgical treatment of peripheral nerve disorders. *Neuroimaging Clin N Am* 2004;14:115–33.
- Hein PA, Eskey CJ, Dunn JF, Hug EB. Diffusion-weighted imaging in the follow-up of treated high-grade gliomas: tumor recurrence versus radiation injury. *Am J Neuroradiol* 2004;25:201–9.
- Jarvik JG, Yuen E. Diagnosis of carpal tunnel syndrome: electrodiagnostic and magnetic resonance imaging evaluation. *Neurosurg Clin N Am* 2001;12:241–53.
- Jarvik JG, Kliot M, Maravilla KR. MR nerve imaging of the wrist and hand. *Hand Clin* 2000;16:13–24 vii.
- Jarvik JG, Yuen E, Kliot M. Diagnosis of carpal tunnel syndrome: electrodiagnostic and MR imaging evaluation. *Neuroimaging Clin N Am* 2004;14:93–102 viii.
- Jones DK, Horsfield MA, Simmons A. Optimal strategies for measuring diffusion in anisotropic systems by magnetic resonance imaging. *Magn Reson Med* 1999a;42:515–25.
- Jones DK, Simmons A, Williams SC, Horsfield MA. Non-invasive assessment of axonal fiber connectivity in the human brain via diffusion tensor MRI. *Magn Reson Med* 1999b;42:37–41.
- Jones DK, Williams SC, Gasston D, Horsfield MA, Simmons A, Howard R. Isotropic resolution diffusion tensor imaging with whole brain acquisition in a clinically acceptable time. *Hum Brain Mapp* 2002;15: 216–30.
- Le Bihan D. Molecular diffusion, tissue microdynamics and microstructure. *NMR Biomed* 1995;8:375–86.
- Le Bihan D, Mangin JF, Poupon C, Clark CA, Pappata S, Molko N, Chabriat H. Diffusion tensor imaging: concepts and applications. *J Magn Reson Imaging* 2001;13:534–46.
- Masutani Y, Aoki S, Abe O, Hayashi N, Otomo K. MR diffusion tensor imaging: recent advance and new techniques for diffusion tensor visualization. *Eur J Radiol* 2003;46:53–66.
- Melhem ER, Mori S, Mukundan G, Kraut MA, Pomper MG, van Zijl PC. Diffusion tensor MR imaging of the brain and white matter tractography. *Am J Roentgenol* 2002;178:3–16.
- Monagle K, Dai G, Chu A, Burnham RS, Snyder RE. Quantitative MR imaging of carpal tunnel syndrome. *Am J Roentgenol* 1999;172: 1581–6.
- Mori S, Crain BJ, Chacko VP, van Zijl PC. Three-dimensional tracking of axonal projections in the brain by magnetic resonance imaging. *Ann Neurol* 1999;45:265–9.
- Pajevic S, Pierpaoli C. Color schemes to represent the orientation of anisotropic tissues from diffusion tensor data: application to white matter fiber tract mapping in the human brain. *Magn Reson Med* 1999; 42:526–40.
- Parker GJ, Wheeler-Kingshott CA, Barker GJ. Estimating distributed anatomical connectivity using fast marching methods and diffusion tensor imaging. *IEEE Trans Med Imaging* 2002;21:505–12.

- Parker GJ, Haroon HA, Wheeler-Kingshott CA. A framework for a streamline-based probabilistic index of connectivity (PICO) using a structural interpretation of MRI diffusion measurements. *J Magn Reson Imaging* 2003;18:242–54.
- Pierpaoli C, Jezzard P, Basser PJ, Barnett A, Di Chiro G. Diffusion tensor MR imaging of the human brain. *Radiology* 1996;201:637–48.
- Poupon C, Mangin J, Clark CA, Frouin V, Regis J, Le Bihan D, Bloch I. Towards inference of human brain connectivity from MR diffusion tensor data. *Med Image Anal* 2001;5:1–15.
- Reese TG, Weisskoff RM, Smith RN, Rosen BR, Dinsmore RE, Wedeen VJ. Imaging myocardial fiber architecture in vivo with magnetic resonance. *Magn Reson Med* 1995;34:786–91.
- Ries M, Jones RA, Basseau F, Moonen CT, Grenier N. Diffusion tensor MRI of the human kidney. *J Magn Reson Imaging* 2001;14:42–9.
- Shimony JS, McKinstry RC, Akbudak E, Aronovitz JA, Snyder AZ, Lori NF, Cull TS, Conturo TE. Quantitative diffusion-tensor anisotropy brain MR imaging: normative human data and anatomic analysis. *Radiology* 1999;212:770–84.
- Sinha U, Yao L. In vivo diffusion tensor imaging of human calf muscle. *J Magn Reson Imaging* 2002;15:87–95.
- Skare S, Hedehus M, Moseley ME, Li TQ. Condition number as a measure of noise performance of diffusion tensor data acquisition schemes with MRI. *J Magn Reson* 2000;147:340–52.
- Skorpil M, Karlsson M, Nordell A. Peripheral nerve diffusion tensor imaging. *Magn Reson Imaging* 2004;22:743–5.
- Stejskal EO, Tanner JE. Spin diffusion measurements: spin echoes in the presence of a time-dependent field gradient. *J Phys Chem* 1965;42:288–92.
- Tench CR, Morgan PS, Blumhardt LD, Constantinescu C. Improved white matter fiber tracking using stochastic labeling. *Magn Reson Med* 2002;48:677–83.
- Weber J, Mattle HP, Heid O, Remonda L, Schroth G. Diffusion-weighted imaging in ischaemic stroke: a follow-up study. *Neuroradiology* 2000;42:184–91.
- Westin CF, Maier SE, Mamata H, Nabavi A, Jolesz FA, Kikinis R. Processing and visualization for diffusion tensor MRI. *Med Image Anal* 2002;6:93–108.
- Wheeler-Kingshott CA, Hickman SJ, Parker GJ, Ciccarelli O, Symms MR, Miller DH, Barker GJ. Investigating cervical spinal cord structure using axial diffusion tensor imaging. *Neuroimage* 2002;16:93–102.
- Wheeler-Kingshott CA, Barker GJ, Steens SCA, van Buchem MA. D: the diffusion of water. In: Tofts P, editor. *Quantitative MRI of the brain: measuring changes caused by disease*. New York: Wiley; 2003. p. 203–56.
- Wieshmann UC, Clark CA, Symms MR, Franconi F, Barker GJ, Shorvon SD. Reduced anisotropy of water diffusion in structural cerebral abnormalities demonstrated with diffusion tensor imaging. *Magn Reson Imaging* 1999;17:1269–74.